



Importance of the Sequence-Directed DNA Shape for Specific Binding Site Recognition by the Estrogen-Related Receptor

Kareem Mohideen-Abdul^{1,2,3,4}, Karima Tazibt^{1,2,3,4}, Maxime Bourguet^{4,5}, Isabelle Hazemann^{1,2,3,4}, Isabelle Lebars^{1,2,3,4}, Maria Takacs^{1,2,3,4}, Sarah Cianfèrani^{4,5}, Bruno P. Klaholz^{1,2,3,4}, Dino Moras^{1,2,3,4} and Isabelle M. L. Billas^{1,2,3,4*}

¹ Centre for Integrative Biology (CBI), Department of Integrated Structural Biology, Institute of Genetics and of Molecular and Cellular Biology (IGBMC), Illkirch, France, ² Centre National de la Recherche Scientifique (CNRS) UMR 7104, Illkirch, France, ³ Institut National de la Santé et de la Recherche Médicale (INSERM) U964, Illkirch, France, ⁴ Université de Strasbourg, Strasbourg, France, ⁵ Laboratoire de Spectrométrie de Masse BioOrganique, Centre National de la Recherche Scientifique (CNRS), IPHC UMR 7178, Strasbourg, France

OPEN ACCESS

Edited by:

Jan-Ake Gustafsson,
University of Houston,
United States

Reviewed by:

Enzo Lalli,
INSERM, France
Andrew C. B. Cato,
Karlsruhe Institute of
Technology, Germany

*Correspondence:

Isabelle M. L. Billas
billas@igbmc.fr

Specialty section:

This article was submitted
to Molecular and Structural
Endocrinology,
a section of the journal
Frontiers in Endocrinology

Received: 31 March 2017

Accepted: 06 June 2017

Published: 20 June 2017

Citation:

Mohideen-Abdul K, Tazibt K,
Bourguet M, Hazemann I, Lebars I,
Takacs M, Cianfèrani S, Klaholz BP,
Moras D and Billas IML (2017)
Importance of the Sequence-Directed
DNA Shape for Specific Binding Site
Recognition by the Estrogen-Related
Receptor.
Front. Endocrinol. 8:140.
doi: 10.3389/fendo.2017.00140

Most nuclear receptors (NRs) bind DNA as dimers, either as hetero- or as homodimers on DNA sequences organized as two half-sites with specific orientation and spacing. The dimerization of NRs on their cognate response elements (REs) involves specific protein–DNA and protein–protein interactions. The estrogen-related receptor (ERR) belongs to the steroid hormone nuclear receptor (SHR) family and shares strong similarity in its DNA-binding domain (DBD) with that of the estrogen receptor (ER). *In vitro*, ERR binds with high affinity inverted repeat REs with a 3-bps spacing (IR3), but *in vivo*, it preferentially binds to single half-site REs extended at the 5'-end by 3 bp [estrogen-related response element (ERREs)], thus explaining why ERR was often inferred as a purely monomeric receptor. Since its C-terminal ligand-binding domain is known to homodimerize with a strong dimer interface, we investigated the binding behavior of the isolated DBDs to different REs using electrophoretic migration, multi-angle static laser light scattering (MALLS), non-denaturing mass spectrometry, and nuclear magnetic resonance. In contrast to ER DBD, ERR DBD binds as a monomer to EREs (IR3), such as the *tff1* ERE-IR3, but we identified a DNA sequence composed of an extended half-site embedded within an IR3 element (embedded ERRE/IR3), where stable dimer binding is observed. Using a series of chimera and mutant DNA sequences of ERREs and IR3 REs, we have found the key determinants for the binding of ERR DBD as a dimer. Our results suggest that the sequence-directed DNA shape is more important than the exact nucleotide sequence for the binding of ERR DBD to DNA as a dimer. Our work underlines the importance of the shape-driven DNA readout mechanisms based on minor groove recognition and electrostatic potential. These conclusions may apply not only to ERR but also to other members of the SHR family, such as androgen or glucocorticoid, for which a strong well-conserved half-site is followed by a weaker one with degenerated sequence.

Keywords: nuclear receptors, estrogen-related receptor, homodimerization, steroid receptors, DNA recognition, DNA shape, minor groove shape recognition

INTRODUCTION

The binding of DNA by nuclear receptors (NRs) is essential for the proper transcriptional regulation of the expression of target genes involved in crucial physiological and metabolic pathways (1–3). Specific DNA recognition encompasses several levels of complexity and involves at first place a direct readout mechanism, where the NRs bind specific genomic sequences, known as response elements (REs) and make sequence-specific contacts with the major groove by the formation of base- and amino acid-specific interactions (4–7). Most NRs bind DNA on their cognate RE, that are composed of two hexanucleotide half-sites, either as homodimers or as heterodimers with the ubiquitous partner RXR. Cooperative dimerization of the NRs on DNA increases the repertoire of binding sites that can be bound in a specific manner and leads to more efficient DNA binding. However, a few NRs can also bind DNA efficiently as monomers (7, 8). In this case, the receptors make use of an additional region of interaction between the C-terminal extension (CTE) of the NR and the 3-bp extension at the 5'-end of the RE. The estrogen-related receptors (ERRs) are orphan NRs that are structurally related to the classical estrogen receptors (ERs) and have been categorized as monomeric receptors (9–11). In fact, the ERRs have a marked preference for the recognition of the sequence TNAAGGTCA, which is referred as the estrogen-related response element (ERRE) and corresponds to the classical 6-bp half-site AGGTCA and a 3-bp 5'-extension TNA, where $N = C$ is the preferred nucleotide (12–14). The ERRs can also bind *in vitro* with high affinity to the inverted repeat 3 (IR3) REs, which are bound by the ERs and are composed of two hexanucleotide half-sites of consensus sequence AGGTCA organized as inverted repeats separated by a 3-bp spacer (15, 16). However, *in vivo*, a very small overlap exists between the set of genes bound by ERRs and ERs, and when it does, direct overlap occurs through an ERRE embedded within an ERE, leading to fine tuning of the expression of a small set of genes (12). The ERRs do bind the genome strongly and in a widespread and ligand-independent manner. The genes controlled by the ERRs are in a large part associated with metabolic and physiological pathways, such as glucose metabolism, mitochondrial activity, and energy sensing. Therefore, the ERRs represent major transcriptional regulators of energy metabolism in response to physiological and/or environmental challenges (17–23).

At the structural level, the understanding of the ERR function has relied on studies of the isolated DNA (DBD) and ligand-binding domains (LBD). A single ERR β DBD structure was solved and showed a monomer bound to a short 13-bp DNA sequence encompassing the 9-bp ERRE (24). On the other hand, the ERR LBD was crystallized as a homodimer (25–29), suggesting that the LBD mediates the main dimerization properties of ERRs. Functional data on full ERRs suggested that the homodimer, and not the monomer, is functionally relevant and capable of interaction with co-regulators, in particular with the coactivator PGC-1. This apparent contradiction between the homodimerization of the full receptor and the identification of monomeric ERR-binding sites represents a puzzling piece of information that has not been elucidated until now. Since the full ERR assembly on DNA engage the DBD which is in principle

able to perform DNA recognition, we decided to focus on the isolated DBD bound to different types of REs. Solution studies of ERR DBD by nuclear magnetic resonance (NMR) showed that the isolated DBD is a monomer in the absence of DNA or in the presence of a short sequence encompassing the 9-bp extended half-site (24, 30). This is also the case with the ER which is a monomer in solution in the absence of DNA, but that dimerizes on a palindromic ERE/IR3 (31). Homodimerization of ERs and of the other steroid receptors [the androgen (AR), glucocorticoid (GR), mineralocorticoid (MR), and progesterone (PR) receptors, so called the oxosteroid receptors] on IR3 is strongly cooperative in the presence of a correctly configured DNA site (4, 5, 32–35). Therefore, we wondered whether ERR DBD could homodimerize on certain DNA-binding sites and explored a large panel of DNA sequences onto which ERR α DBD can bind. Here, we report the results of these studies and we show, by using complementary biophysical and structural techniques, that stabilization of a dimer of ERR α DBD is possible on specific sequences. Several natural sequences of ERR REs have been considered in our analysis, and to gain deeper insight into the key determinants for ERR DBD dimer formation on DNA, we further designed mutant and chimera DNA sequences that helped us in delineating the critical region for the stabilization of the DBD dimer. In particular, we uncovered that the sequence-driven shape of DNA at the level of the site that is potentially bound by the second DBD subunit is essential for such a process. Thus, ERR α DBD uses information in the minor groove to achieve DNA-binding and concomitant dimer stabilization. Since the natural DNA-binding sites of the NRs are often degenerated with respect to the consensus sequence, somehow accounting for their specific transcriptional output, our results provide a nice example of DNA shape recognition and offer perspectives in the understanding of NR DNA recognition.

MATERIALS AND METHODS

Cloning, Protein Expression, and Purification

Mouse mammary ERR α DBD (70–170) was cloned in the in-house expression vector pNEAtH. The vector was transformed in *Escherichia coli* BL21 (DE3) pRARE2 strain, grown at 37°C and induced for protein expression at OD_{600nm} = 0.6 with 1 mM IPTG at 25°C for 3 h. The cell pellet was resuspended in binding buffer (20 mM Tris pH = 8.0, 400 mM NaCl, 10% glycerol, 4 mM CHAPS) and lysed by sonication. The crude extract was centrifuged at 45,000 $\times g$ for 1 h at 4°C. The lysate was loaded on a Ni affinity step on HisTrap FF crude column (GE Healthcare, Inc.), and the protein was eluted at a concentration of 150 mM imidazole. The hexahistidine tag was cleaved overnight using thrombin protease. ERR α -DBD was subjected to a Heparin column using an increasing salt gradient. Finally, the ERR α -DBD was polished by size-exclusion chromatography (SEC) in a SEC buffer (50 mM Bis Tris pH = 7.0, 120 mM KCl, 0.5 mM CHAPS, 4 mM MgCl₂) by using a Superdex S75 16/60 column (GE Healthcare). Complexes were formed by mixing the appropriate DNA solution to the purified ERR α DBD to achieve desired DNA:protein molar ratios. The

complex was incubated at least 30 min at 4°C before performing the respective experiments.

DNA Annealing

HPLC purified single-stranded DNAs were ordered from Sigma-Aldrich, Inc. or Euromedex France. The single-stranded DNA oligonucleotide and its respective anti-sense DNA fragment were mixed in the DNA annealing buffer (10 mM Tris pH = 8.0, 100 mM NaCl, 1% DMSO, 0.1 mM EDTA), heated at 95°C, and gradually cooled down to 4°C using a BIO-RAD PCR machine. 4 mM MgCl₂ was added to the cooled annealed DNA sample.

Polyacrylamide Native Gel Electrophoresis

The protein–DNA complexes were run on an 8% polyacrylamide gel (PAGE) at 2 W constant power after pre-running the gel for 40 min at 4°C. Two different native gel systems were used (i) Tris/CAPS (pH = 9.4) buffer system contained 60 mM Tris base and 40 mM CAPS (3-cyclohexyl-amino-1-propane-sulfonic acid) (ii) Ammonia/CAPS buffer (pH = 10.4) system (containing 37 mM ammonia and 60 mM CAPS). Approximately 3–5 μg protein was loaded per lane along with its DNA counterpart at defined molar ratios. The polyacrylamide gels were stained using Instant Blue Protein Stain (Expedeon Protein Solutions) for 15 min and rinsed in water.

SEC Coupled to Multi-Angle Laser Light Scattering

Size-exclusion chromatography (SEC)-MALLS/QELS experiments were performed on a multi-angle laser light scattering detector (miniDAWN TREOS, Wyatt Technologies) coupled in-line with SEC and an interferometric refractometer (Optilab T-rEX, Wyatt Technologies). A Superdex S75 or S200 10/300 GL column (total volume 24 mL, GE Healthcare) with a flow rate of 0.5 mL/min was used to separate the sample before performing the MALLS/QELS measurement. Experiments were done with 50–100 μL receptor–DNA complex samples at concentrations between 1 and 3 mg/mL in 20 mM Bis Tris pH = 7.0, 120 mM KCl, 1 mM MgCl₂, 0.5 mM CHAPS, 1 mM TCEP. The molar mass was determined by construction of Debye plot using Zimm formalism [plot of $K^*c/R(\theta)$ as a function of $\sin^2(\theta/2)$] at 1-s data interval. The analysis of the data was performed using the ASTRA 6.1 software (Wyatt Technologies).

Native Electrospray Ionization Mass Spectrometry

Native nano-Electrospray-Mass Spectrometry (nanoESI-MS) analyses were performed on an electrospray quadrupole-time-of-flight mass spectrometer (Synapt G2 HDMS, Waters, Manchester, UK) coupled to an automated chip-based nanoESI source (Triversa Nanomate, Advion, Ithaca, NY, USA). The mass spectrometer was calibrated using singly charged ions produced by a 2-g/L solution of cesium iodide (Acros organics, Thermo Fisher Scientific, Waltham, MA, USA) in 2-propanol/water (50/50 v/v). Samples were buffer exchanged in 150 mM ammonium acetate (NH₄Ac), pH 7.1 buffer using 0.5 mL Zeba™ Spin desalting Columns (Thermo Fisher Scientific, Waltham,

MA, USA) and centrifuged at 1,500 × g for 2 min. After buffer exchange, concentrations were determined by UV-Vis using a Nanodrop 2000 Spectrophotometer (Thermo Fisher Scientific, Waltham, MA, USA). Samples were diluted to 5 μM in 150 mM ammonium acetate, pH = 7.1 buffer and directly infused into the mass spectrometer. Instrumental parameters were optimized for the detection of labile non-covalent complexes by raising the interface pressure to 6 mbar and the cone voltage to 140 V. Data treatment was realized with MassLynx 4.1 software (Waters, Manchester, UK).

Nuclear Magnetic Resonance

Nuclear magnetic resonance experiments were recorded at 700 MHz on an Avance III Bruker spectrometer equipped with a TCI z-gradient cryoprobe. NMR data were processed using TopSpin (Bruker) and analyzed with Sparky software packages (36). NMR experiments were performed in 50 mM sodium phosphate buffer (pH 7.0), 5 mM MgCl₂, and 1 mM TCEP in 90/10 H₂O/D₂O. PAGE-purified DNAs were annealed by heating at 95°C and snap-cooled at 4°C. The concentration of DNA samples was measured using a Nanodrop Spectrometer and calculated with molar extinction coefficients. DNA samples volumes were 150 μL in 3-mm NMR tubes. ¹H assignments were obtained using standard homonuclear experiments. NMR data were acquired at 15°C and 20°C. Solvent suppression was achieved using the “Jump and Return” sequence combined to WATERGATE (37–39).

Two-dimensional NOESY spectra were acquired with mixing time of 400 and 50 ms. Base pairing was established *via* sequential nuclear Overhauser effects (NOEs) observed in 2D NOESY spectra at different mixing times. Complexes were formed by stepwise addition of ERRα DBD to 100 μM DNA samples, to achieve DNA:protein ratios of 0.5, 1.0, 1.5, and 2.0. The concentrations of protein samples ranged from 0.8 to 1.4 mM maintaining minimal dilution of the DNA samples. All titrations experiments were performed at 20°C, monitoring the imino protons region of 1D spectra.

RESULTS

Polyacrylamide Native Gels Suggest the Existence of Different ERR–DNA Complexes Depending on the Nature of the DNA Sequence

Estrogen-related receptor binds to IR3 REs encompassing two 6 bps DNA-binding sites separated by 3 bps, as well as to 9 bps extended half-site REs composed of a single specific DNA-binding site of the type TNAAGGTCA (ERRE), the latter REs representing most of the natural REs found in target gene promoters. Here, we first address the issue of complex formation of ERRα DBD–DNA for an extended range of DNA targets, using polyacrylamide Ammonia/CAPS or Tris/CAPS native gel electrophoresis. We considered 33 bp DNA fragments originating from the *tralpha* (*tra*) and *lactoferrin* (*lf*) (40, 41) gene promoters (Table S1 in Supplementary Material) as representatives of specific natural ERREs (**Figure 1A**) and reconstituted

complexes between ERR α DBD and DNA using increasing ratios of protein to DNA. For these two different natural ERREs, the ERR α DBD-ERRE complexes migrate as a single band. In addition, we considered two *tra* ERRE fragments of different length, a short one of 13 bp only that solely encompasses the extended 5'-TGAAGGTCA-3' motif, where only one DBD subunit is allowed to bind and a longer one with 29 bps, which would potentially allow the binding of a DBD dimer (Figure 1B). We observed a single migration band for the 13- and 29-bp ERRE complexes, irrespective of the ratio between DNA and the DBD, from sub-stoichiometric (1:0.5) to higher ratios (up to 1:4). This suggests that a monomer is bound to the 13-bp DNA fragment and remains monomeric in the case of longer DNA fragments

(as shown with 29 and 33 bps). No potential dimer formation seems to occur when the amount of DBD subunits is increased. When comparing the migration of ERR α DBD on the ERE/IR3 of the *tff1* gene promoter (16, 42) (*tff1* ERE-IR3) with that of ERR α DBD-*tra* ERRE, a similar migration pattern is observed, suggesting a monomer on this IR3 RE (Figure 1C, lanes 1, 2). In contrast, when considering a composite element made of an extended half-site ERRE embedded into an IR3 RE (embERRE/IR3), we observed a delayed migration of the complex into the gel (Figure 1C, lanes 3, 5). Similarly, when the ratio between the embERRE/IR3 (26 bps here) and DBD is increased, from stoichiometric (DNA:protein = 1:0.25) to higher ratios (up to 1:4), the low migration band disappears and a higher migration band

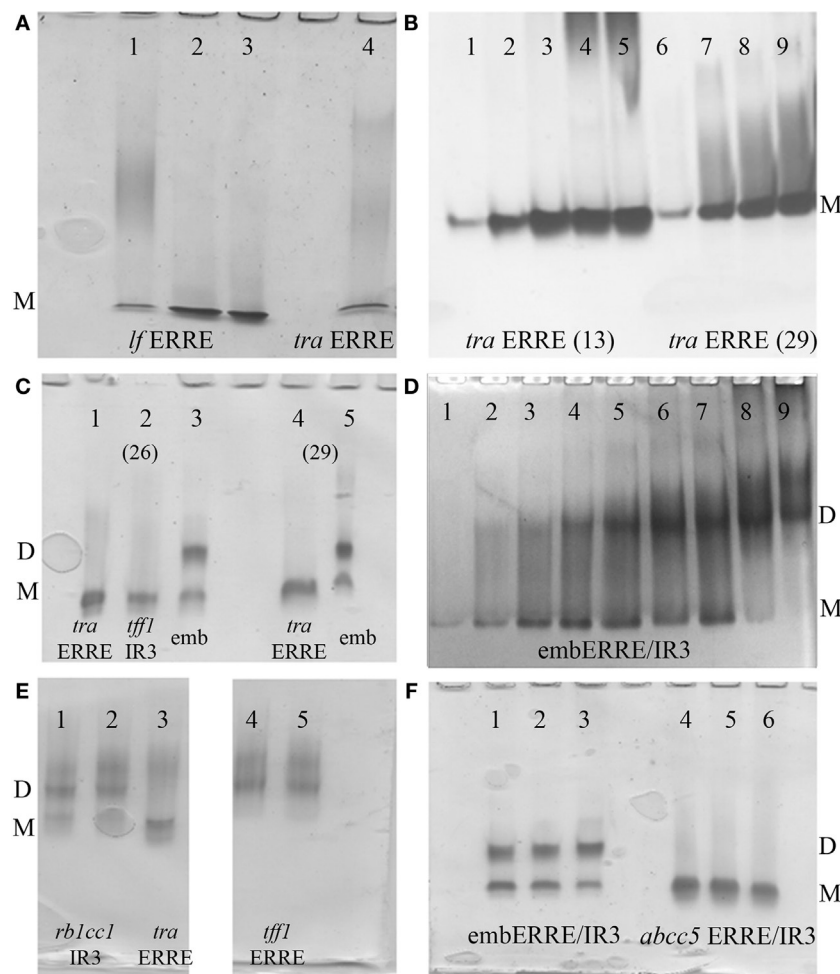


FIGURE 1 | Polyacrylamide native gels. **(A)** Ammonia/CAPS polyacrylamide gel of ERR α DBD-*lf* estrogen-related element (ERRE) (lanes 1–3) for different DNA:protein ratios 1:1, 0.5:1, and 0.25:1 compared to ERR α DBD-*tra* ERRE DNA:protein ratio = 0.25:1 (lane 4), showing the existence of the monomer only on DNA. **(B)** Effect of DNA length on complex formation for ERR α DBD-*tra* ERRE with 13 bps (lane 1–5) and 29 bps (lane 6–9) for different molar ratios of DNA:DNA-binding domain (DBD), 1:0.5 (lanes 1, 6), 1:1 (lanes 2, 7), 1:2 (lanes 3, 8), 1:3 (lanes 4, 9), and 1:4 (lane 5). **(C)** ERR α DBD complexes were formed with 26-bp DNA fragments of *tra* ERRE (lane 1), *tff1* ERE/IR3 (lane 2), and embERRE/IR3 (lane 3) and with 29-bp fragments of *tra* ERRE (lane 4) and embERRE/IR3 (lane 5) with a molar ratio of DNA:DBD of 1:1. **(D)** ERR α DBD-embedded ERRE/IR3 complexes. Different ratios of DNA:protein were considered for complex formation with the 26 bp fragment originating from the embERRE/IR3 response elements (lanes 1–9: increasing DNA:protein ratios 1:0.25, 1:0.5, 1:1, 1:1.5, 1:2, 1:2.5, 1:3, 1:3.5, and 1:4); showing the appearance of the dimer on DNA. **(E)** Dimer formation is not restricted to the DNA sequence embERRE/IR3, as shown for *rb1cc1* IR3 (lanes 1, 2, ratios 1:1 and 0.5:1, respectively) and *tff1* ERRE (lanes 4, 5, ratios 1:1 and 0.5:1, respectively) as compared to the strict monomer observed on *tra* ERRE (lane 3, ratio 1:1). **(F)** Comparison of complexes formed between ERR α DBD and embedded ERRE/IR3 DNA sequences, such as embERRE/IR3 (lanes 1–3) and *abcc5* ERRE/IR3 (lanes 4–6) for three different ratios of DNA:DBD (1:1, 0.5:1, and 0.25:1). In all panels, M and D stand for monomer and dimer, respectively.

is observed (Figure 1D). These data suggest that a different type of ERR α DBD–DNA complex can be formed on the embERRE/IR3 sequence, as compared to the monomeric ERR α DBD–*tra* ERRE, –*lf* ERRE or –*tff1* ERE–IR3 complexes and likely corresponds to dimeric ERR α DBD on DNA. To gain insight into the unexpected behavior of ERR α DBD on the embERRE/IR3 sequence, we explored more sequences belonging to either the IR3-type of REs or to the natural extended ERREs. We found diversity in the migration pattern inside each of the two different types, as shown for *tff1* ERE–IR3 (16, 42) and the *rb1cc1* IR3 (43) as examples of IR3-binding sites, or *tra* ERRE and *tff1* ERRE as examples of ERRE natural DNA REs (Figures 1C,E). While the *tff1* ERE–IR3 and the *tra* ERRE result into a single low migration band, the *rb1cc1* IR3 and the *tff1* ERRE give a more complex migration pattern with mainly two bands, a lower migration band and a delayed migration band similar to what is observed in the case of ERR α DBD–embERRE/IR3. On the other hand, different embedded ERRE/IR3 REs do not necessarily lead to the observation of two migrating species, as shown in Figure 1F, for the natural ERRE/IR3 RE of the *abc5* gene promoter. Altogether, these data suggest that the existence of a single monomeric species or the occurrence of higher molecular complexes, possibly dimer, on DNA strongly depends on the exact nature of the DNA sequence. In fact, the DNA sequence is likely to be the key factor for the stabilization of ERR α DBD dimer on DNA.

Electrospray Ionization Mass Spectrometric Analysis Shows the Existence of ERR α DBD Dimer on the Embedded ERRE/IR3

Based on our results obtained from native polyacrylamide gels, we wish to assess the exact binding stoichiometry of ERR α DBD on different DNA sequences and first relied on electrospray mass spectrometry (ESI-MS) analysis carried out under non-denaturing conditions. The mass measurement ($29,737 \pm 1$ Da) indicates that the complex between ERR α DBD and *tra* ERRE is composed of a single DBD subunit on the DNA sequence (Figure 2A; Table S2 in Supplementary Material). When ERR α DBD–embERRE/IR3 complexes are considered, MS analysis indicate not only the presence of a monomer but also of a dimer of ERR α DBD on this RE whatever the length of the latter sequence (29 and 33 bps in Figures 2B,C), see Table S1 in Supplementary Material for the measured masses and Table S2 in Supplementary Material for the measured masses. The results of the MS analysis are consistent with the biochemical data from the native gel electrophoresis and allow the attribution of the two migration bands observed in the native gels for these complexes as the monomeric and the dimeric ERR α DBD–DNA species. MS analysis further suggests that ERR α DBD can also form a dimer on the IR3 RE of the *rb1cc1* gene promoter (Figure 2D), suggesting that the presence of a dimer is

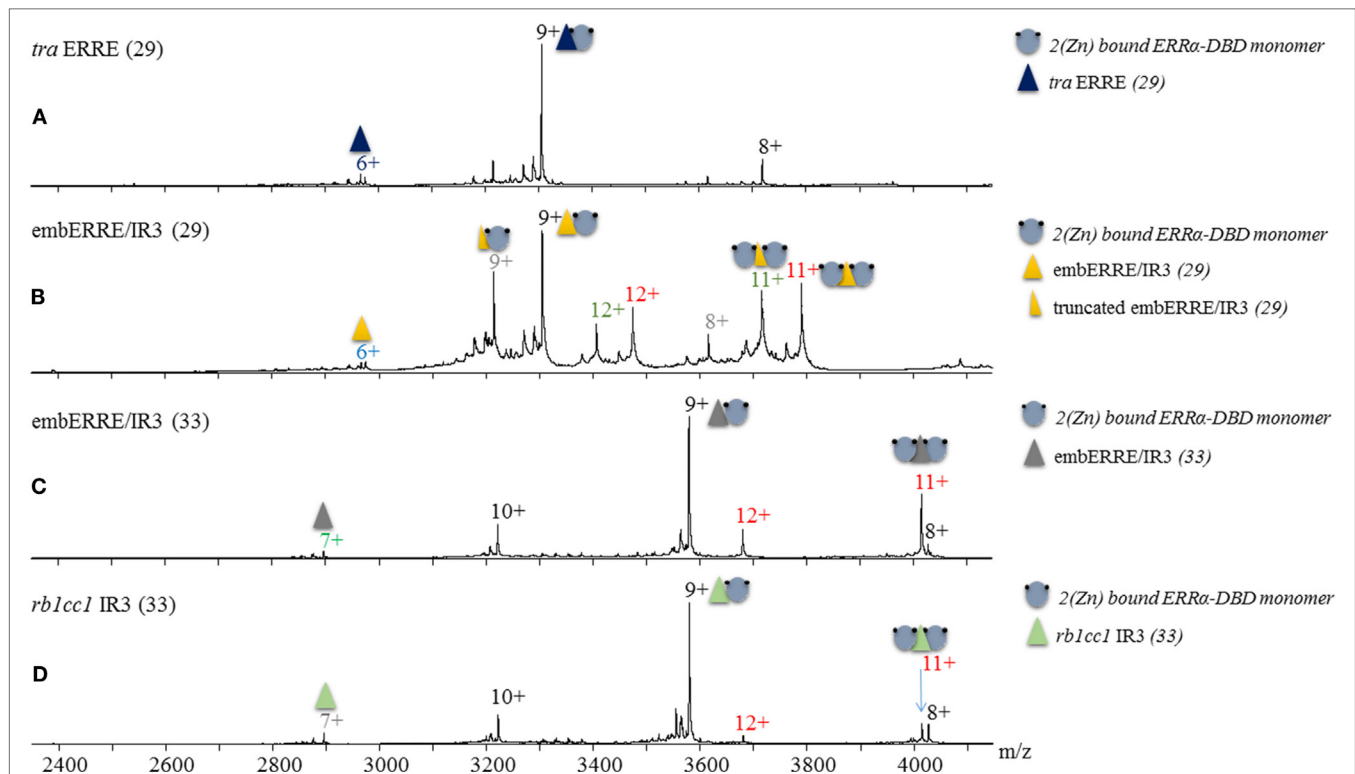


FIGURE 2 | Non-denaturing Mass Spectrometry analysis of ERR α DNA-binding domain (DBD)–DNA complexes. Electrospray ionization mass spectra obtained in non-denaturing conditions of (A) ERR α DBD–*tra* estrogen-related element (ERRE), (B) ERR α DBD–embERRE/IR3 (29), (C) ERR α DBD–embERRE/IR3 (33), (D) ERR α DBD–*rb1cc1* IR3 complexes. The different charged states of the monomeric and dimeric ERR α DBD–DNA complexes are given in black and red, respectively, above the *m/z* peaks. In panel (B), two more species are observed corresponding to DBD monomer (charged state in gray) and dimer (charged state in green) on a truncated DNA lacking one base pair. In all spectra, a small fraction of free DNA is observed (at *m/z* of around 2,900).

not limited to the embedded RE emberERRE/IR3, an observation fully confirmed by the other techniques used in this study.

SEC Coupled to Multi-Angle Laser Light Scattering Suggests an Equilibrium between Dimer and Monomer Species for Some ERR α DBD–DNA Complexes

Mass spectrometric results suggest the existence of monomeric and dimeric ERR α DBD species on the embedded ERRE/IR3 REs and native gels indicate that the existence of larger, possibly dimeric species is not limited to this specific RE, but to other DNAs, as shown for *rb1cc1* IR3 and *tff1* ERRE. Since mass spectrometric analysis in non-denaturing conditions is performed in ammonium acetate, we decided to undertake multi-angle laser light scattering experiments (MALLS) coupled to SEC in more physiological buffer conditions. SEC-MALLS allows the quantitative in-line measurements of the molar mass of the species in solution that are first separated on a SEC column. We first considered ERR α –DBD complexes with 26-bps DNA fragment of either *tra* ERRE, *tff1* ERE/IR3, or emberERRE/IR3 and added a rather large excess of DNA while reconstituting the complexes, resulting in a chromatogram with two overlapping peaks, one belonging to the DBD–DNA complex and the other one, on the right, to the free DNA. As shown in **Figure 3A**, the two complexes ERR α DBD–*tra* ERRE and ERR α DBD–*tff1* ERE/IR3 are composed of one monomer on DNA, while the measured molar mass of ERR α DBD–emberERRE/IR3 corresponds to the mass of the dimer. As observed in the native gels (**Figure 1F**) and shown in **Figure 3B**, ERR α DBD is a monomer on the embedded ERRE/IR3 RE of the *abcc5* gene promoter. While the binding stoichiometry of all the complexes was rather unambiguous, we wondered how the complexes between ERR α DBD and *rb1cc1* IR3 or *tff1* ERRE would behave since we saw that their migration pattern on the gels was rather complex. As shown in **Figure 3C**, these measured molar mass of the two complexes reflects the coexistence of dimer (at the left-hand side of the SEC peak) and monomer (toward the center of the peak) on DNA. This suggests that the dimer is less stable on these DNAs when compared to emberERRE/IR3 and that both species are in equilibrium in solution. The results of SEC-MALLS experiments are thus consistent with ESI-MS data, and strongly suggest that the dimerization of the isolated ERR α DBD on DNA is possible, but strongly depends on the DNA sequence of the target binding site.

Binding Properties of ERR α DBD onto DNAs Investigated by NMR

Nuclear magnetic resonance was used to investigate the binding properties of ERR α DBD onto different types of DNA: *tff1* ERE/IR3, *lf* ERRE, *tra* ERRE, *rb1cc1* IR3, and emberERRE/IR3. NMR spectra display imino protons resonances (found between 12 and 14 ppm) provided that they are protected from exchange with the solvent. Their observation indicates that the corresponding protons are involved in hydrogen bonds, generally due to the formation of base pairs. All base paired imino protons of free DNAs were first assigned *via* sequential NOEs observed in 2D NOESY

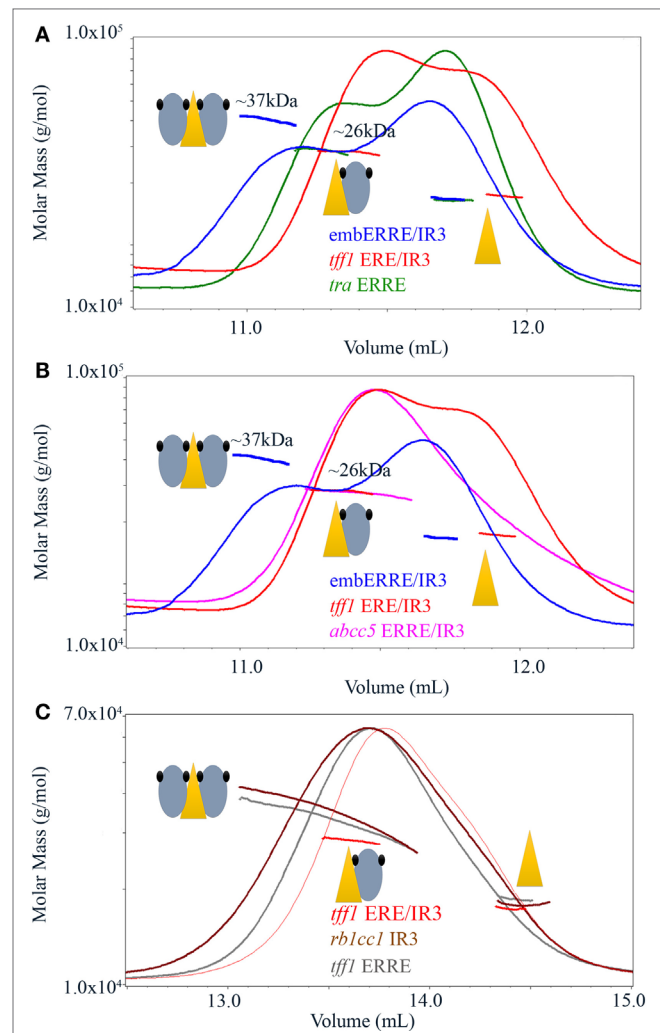


FIGURE 3 | Size-exclusion chromatography-coupled multi-angle laser light scattering of ERR α DNA-binding domain (DBD)–DNA complexes. **(A)** Size-exclusion chromatography (SEC)-MALLS analysis of ERR α DBD bound to emberERRE/IR3(26), *tff1* ERE/IR3(26), and *tra* estrogen-related response element (ERRE) (26) (160 μ M) showing the elution profile on a SEC S75 10/300 with the direct molar mass measurement of each elution peak. ERR α DBD elutes as a dimer for emberERRE/IR3(26) with a measured molar mass of around 37 kDa and as a monomer for *tra* ERRE(26) and *tff1* ERE/IR3(26) with a measured molar mass of 26 kDa. An excess of the 26 bp DNA fragment is seen at the right-hand side of the elution profile. **(B)** SEC-MALLS analysis of ERR α DBD bound to emberERRE/IR3(26), *tff1* ERE/IR3(26), and *abcc5* ERRE/IR3(26) (160 μ M) showing the elution profile on a SEC S75 10/300 with the direct molar mass measurement of each elution peak. ERR α DBD elutes as a dimer for emberERRE/IR3 with a measured molar mass of around 37 kDa, while the embedded *abcc5* ERRE/IR3 elutes as a monomer like *tff1* ERE/IR3(26) with a measured molar mass of 26 kDa. An excess of the 26 bp DNA fragment is seen at the right-hand side of the elution profile. **(C)** SEC-MALLS analysis of ERR α DBD bound to *tff1* ERE/IR3(26), *rb1cc1* IR3(26), and *tff1* ERRE(26) (100 μ M) showing the elution profile on a SEC S200 10/300 with the direct molar mass measurement of each elution peak. In contrast to ERR α DBD–*tff1* ERE/IR3(26) that elutes as a monomer with a measured molar mass of 26 kDa, ERR α DBD bound to *rb1cc1* IR3(26) and *tff1* ERRE(26) shows a molar mass that varies along the elution profile from the mass of the dimer on DNA (left) to that of the monomer on DNA (toward the center of the peak). An excess of the 26 bp DNA fragment is seen at the right-hand side of the elution profile.

(**Figure 4**). The A:T Watson–Crick base pair were discriminated from G:C base pair by the strong correlation observable between T H3 imino proton and the H2 proton of adenine. In a G:C Watson–Crick base pair, two strong NOEs are observable between the guanine H1 and the cytosine amino protons. The chemical shifts of imino protons in 1D spectra were then monitored as a function of ERR α DBD concentration and were used to map the DNA regions in contact with the protein. Complexes were formed by stepwise addition of ERR α DBD to DNAs. Successive additions of ERR α DBD on DNAs resulted in several changes in the imino protons region. Addition of ERR α DBD to *tff1* ERE/IR3 DNA induces chemical shifts of the resonances corresponding to T3, T46, G42, and G48 imino protons, indicating that the protein binds the first extended site. In contrast, the resonances corresponding to T16 and T32 imino protons remain unaffected, suggesting that ERR α DBD does not bind the second site (**Figure 4A**; Figure S1 in Supplementary Material). With *lf* ERRE DNA, most of spectral changes involve nucleotides located in the first extended site. Seven imino protons, T3, T10, T13, T41, G42, T46, and G51 undergo clear chemical shifts, while resonances corresponding to G25, T29, and T32 remain unchanged (**Figure 4B**; Figure S2 in Supplementary Material). These observations indicate that ERR α DBD binds only the first site. The ERR α DBD titration performed on *tra* ERRE DNA also induces changes in the imino protons region. Despite the complexity of the spectra due to overlapping of several resonances, clear chemical changes are observable for T2, G8, G9, G42, and G48 residues, while G21 and G28 do not undergo variations (**Figure 4C**; Figure S3 in Supplementary Material). This suggests that ERR α DBD binds the first extended site and not the second. With *rb1cc1* IR3 DNA, similarly to *tra* ERRE DNA, due to overlapping of resonances, we only considered the imino protons that were well resolved. Addition of ERR α DBD to *rb1cc1* IR3 DNA induces a clear chemical shift of the resonance corresponding to G5 and G36 residues (**Figure 4D**; Figure S4 in Supplementary Material), indicating that the protein contacts the two sites. Finally, titration performed on *emberRE/IR3* DNA also induces perturbations in the imino protons region of 1D spectra. Resonances corresponding to T21, T2, T4, T10, T16, T35, and T41 undergo clear chemical shifts upon ERR α DBD binding (**Figure 4E**; Figure S5 in Supplementary Material). This shows unambiguously that ERR α DBD binds the two sites within the *emberRE/IR3* DNA. Taken together, NMR data suggest that the binding of ERR α DBD affects the first extended site in *tff1* ERE/IR3, *lf* ERRE, and *tra* ERRE DNAs, while the protein binds two sites in the case of *rb1cc1* IR3 and *emberRE/IR3* DNAs, in perfect agreement with the other biophysical and biochemical data.

DNA Chimeras to Delineate the Key Molecular Determinants of ERR Dimerization

For some of the DNA sequences, the ERR α DBD can bind a dimer. This is clearly observed for *emberRE/IR3*, and to some extent for *tff1* ERRE and *rb1cc1* IR3, but neither for the *tff1* ERE/IR3 nor for *tra* ERRE. Thus, the question arises as to which region is key for the stabilization of a DBD dimer on DNA, since the mere presence

of two half-sites is not enough to explain dimerization. Therefore, we considered two DNA sequences, one which is always bound by a monomer (*tff1* ERE/IR3) and another one (*emberRE/IR3*) which leads to dimer stabilization. We then considered chimeras of these two DNA-binding sequences (**Figure 5A**), where the 5' region, including the flanking region and the first half-site belongs to one of the sequence, whereas the 3' region, including the spacer, the second half-site and the flanking region comes from the other DNA. This results into two chimeras, 5'-*tff1* ERE/IR3_3'-*emberRE/IR3* (5'**tff**) and 5'-*emberRE/IR3*_3'-*tff1* ERE/IR3 (5'**emb**). The native ammonia/CAPS native gels of the ERR α DBD–DNA complexes indicate that the two chimeras behave differently. The ERR α DBD–5'**emb** (**Figure 5B**, lanes 5, 6) behaves as a monomer on DNA, in a way similar to ERR α DBD–*tff1* ERE/IR3 (**Figure 5B**, lanes 3, 4), while the ERR α DBD–5'**tff** (**Figure 5B**, lanes 7, 8) allows the formation of a dimer on DNA, like *emberRE/IR3* (**Figure 5B**, lanes 1, 2). SEC-MALLS experiments confirmed these observations (**Figure 5C**), where the measured molar masses for the peak are close to the expected values of the monomer or the dimer on DNA. Similarly, the MS analysis performed under non-denaturing conditions confirmed the existence of dimeric species for both ERR α DBD–*emberRE/IR3* and ERR α DBD–5'**tff** complexes (**Figure 5D**; Table S2 in Supplementary Material). For the latter samples, we noticed that an additional species is present that corresponds to two concatenated DNA molecules. These species come from the initial preparation of DNA (as shown in Figure S6 in Supplementary Material). Taken together, the analysis of the chimeras indicate that the key elements in the DNA sequence for the binding of an ERR α DBD dimer are located in the 3' region and cannot be attributed to the 5' 3bp extension present in the *emberRE/IR3* sequence.

The Sequence of the 3'-End Region of DNA Is Crucial for Dimer Stabilization

In order to get a more detailed molecular insight into the key determinants of ERR α DBD dimerization on DNA, we hypothesized that the 3'-region that differs between *tff1* ERE/IR3 and *emberRE/IR3* is crucial for dimer binding and designed a series of mutants in this region (**Figure 6A**). The nucleotides at positions +7 to +10 that include the last base pair of the half-site and the flanking region differ between *tff1* ERE/IR3 and *emberRE/IR3*. The sequence at these positions is C/G rich with A/T at position +7 for *tff1* ERE/IR3, while for *emberRE/IR3* it is composed of three T/A base pairs followed by A/T. This suggests that the complementary strand of *emberRE/IR3* between position +5 and +9 contains only purines (+5-GGAAA+9), while the related sequence of *tff1* ERE/IR3 is G rich with a T in the middle of the stretch at position +7 (+5-GGTGG+9). Therefore, we first changed the (+5-GGAAA+9) stretch of *emberRE/IR3* to (+5-GGTGG+9), resulting in the *destabPu-emberRE/IR3* (**destabPu**) DNA sequence. In parallel to this, the *tff1* ERE/IR3 GGTGG was modified to GGAAA to mimic locally the sequence seen in *emberRE/IR3*, leading to *tff1* ERE/IR3-Pu sequence (**Pu**). A significant destabilization of dimer formation is observed for the ERR α DBD–*destabPu* complex, as seen in the native polyacrylamide

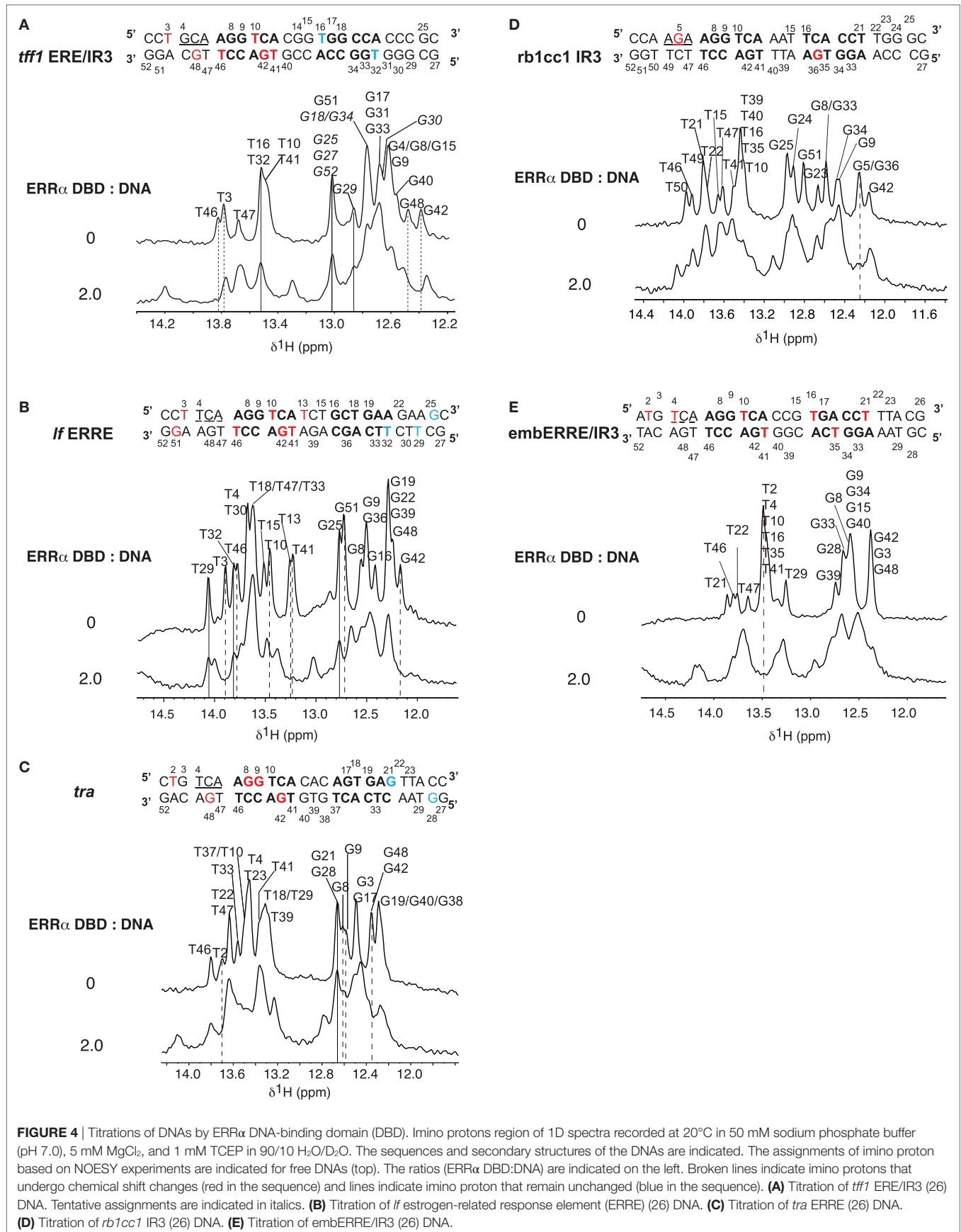


FIGURE 4 | Titrations of DNAs by ERRα DNA-binding domain (DBD). Imino protons region of 1D spectra recorded at 20°C in 50 mM sodium phosphate buffer (pH 7.0), 5 mM MgCl₂, and 1 mM TCEP in 90/10 H₂O/D₂O. The sequences and secondary structures of the DNAs are indicated. The assignments of imino proton based on NOESY experiments are indicated for free DNAs (top). The ratios (ERRα DBD:DNA) are indicated on the left. Broken lines indicate imino protons that undergo chemical shift changes (red in the sequence) and lines indicate imino proton that remain unchanged (blue in the sequence). **(A)** Titration of *tff1* ERE/IR3 (26) DNA. Tentative assignments are indicated in italics. **(B)** Titration of *If* estrogen-related response element (ERRE) (26) DNA. **(C)** Titration of *tra* ERRE (26) DNA. **(D)** Titration of *rb1cc1* IR3 (26) DNA. **(E)** Titration of *embERRE*/IR3 (26) DNA.

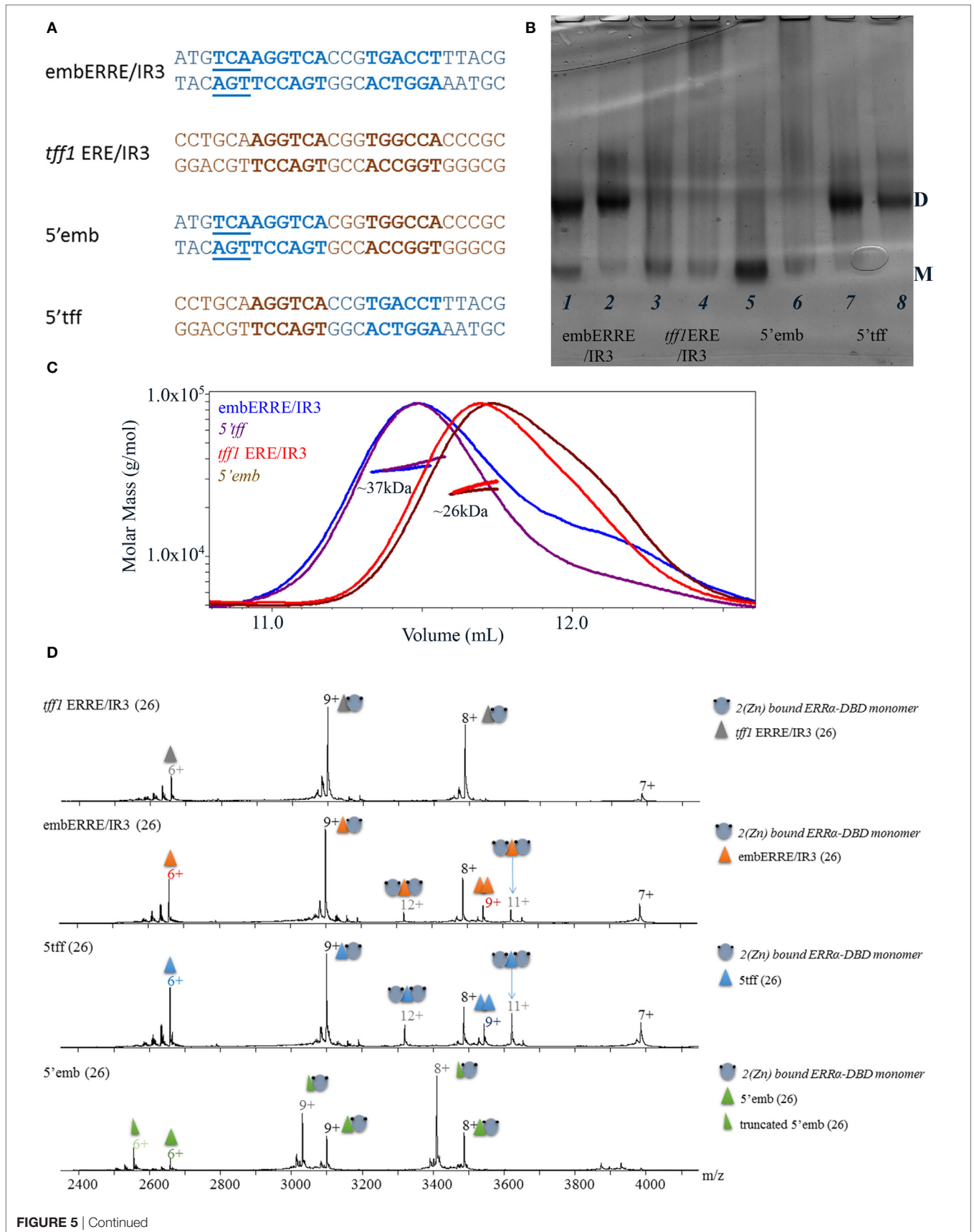


FIGURE 5 | Continued

Biochemical and biophysical analysis of DNA chimeras to delineate structural determinant of dimerization. **(A)** Nucleotide sequence of the 26 bp DNA fragments, including the sequence of the embERRE/IR3 (blue), *tff1* ERE/IR3 (brown), 5'emb (5'-end of embERRE/IR3 and spacer and 3'-end of *tff1* ERE/IR3), and 5'tff (5'-end of *tff1* ERE/IR3 and spacer and 3'-end of embERRE/IR3). **(B)** Ammonia/CAPS polyacrylamide gel of the complexes for two different ratios of DNA:protein (1:1 and 0.25:1) for embERRE/IR3 (lanes 1, 2), *tff1* ERE/IR3 (lanes 3, 4), 5'emb (lanes 5, 6), and 5'tff (lanes 7, 8). **(C)** Size-exclusion chromatography (SEC)-MALLS analysis of ERR α DNA-binding domain (DBD) bound to embERRE/IR3 (blue), *tff1* ERE/IR3 (red), 5'tff (magenta), and 5'emb(brown) (160 μ M) showing the elution profile on a SEC S75 10/300 with the direct molar mass measurement of each elution peak. ERR α DBD elutes as a dimer for embERRE/IR3 and 5'tff with a measured molar mass of around 37 kDa and as a monomer for *tff1* ERE/IR3 and 5'emb with a measured molar mass of 26 kDa. **(D)** Non-denaturing mass spectrometry analysis of ERR α DBD-DNA complexes for (from top to bottom) *tff1* ERE/IR3, embERRE/IR3, 5'tff, and 5'emb, all being 26-bp long. The different charged states of the monomeric and dimeric ERR α DBD-DNA complexes are given in black and gray, respectively, above the *m/z* peak. In all spectra, a small fraction of free DNA and free DNA dimer is observed (at *m/z* of around 2,900).

gel when comparing the intensity of the dimer band with that of ERR α DBD-embERRE/IR3 (**Figure 6B**, lanes 2, 5) and measured with SEC-MALLS (**Figure 6C**), where the SEC peak is shifted to the lower mass range (arrow in **Figure 6C**). However, the sample fraction collected under the maximum of the SEC peak and run on a native gel indicates that some dimer is present in the sample (lane 5 in **Figure 6D**). Even more remarkable is the presence of a slight amount of dimer for ERR α DBD-Pu, while the complex with the parent *tff1* ERE/IR3 DNA only shows monomer on DNA (**Figure 6B**, lanes 6, 9), strongly suggesting that this is the critical region for the stabilization of the second subunit and the dimer formation. The SEC-MALLS of the ERR α DBD-Pu sample shows that the majority of the complexes is composed of monomer on DNA (Figure S7 in Supplementary Material), and no dimer band is seen after the SEC step (**Figure 6D**, lane 8), suggesting that the stabilization of the dimer is weak on this sequence. We tried to be even more conservative in changing the sequence by mutating only one bp in either *tff1* ERE/IR3 DNA or embERRE/IR3. We chose to mutate the base pair at position (+7) from A/T to T/A for *tff1* ERE/IR3 (**IR3mutA7T**) and from T/A to A/T for embERRE/IR3 (**embmutT7A**) (**Figure 6A**). The consequences of this mutation are that the complementary DNA stretch between positions (+5) and (+9) becomes GGAGG for IR3mutA7T and GGTA A for embmutT7A. This mutation has already remarkable effects on the dimer association, either slightly destabilizing the dimer for embERRE/IR3 (**Figure 6B**, lane 8 compared to lane 2 and **Figure 6C**) or promoting a slight dimer association for *tff1* ERE/IR3 (**Figure 6B**, lane 10 compared to lane 9). Notice that the effect persists upon SEC-MALLS measurements and sample collection at the peak maximum (**Figure 6D**, lanes 6, 7). This change in the nature of the nucleotides, either by breaking or restoring the purine stretch observed in the complementary strand between positions (+5) and (+9) is critical. Notice that no dimer is seen to appear, when a TAA extension is present at the 5' end of the second half-site (**3'IR3TAA**) (on the complementary strand and shown in **Figure 6B**, lane 7). Altogether, the data from native polyacrylamide gels and SEC-MALLS suggest that small variations in the DNA sequence at the 3' end are linked to the propensity of the DBD to dimerize. Thus, subtle variations in the sequence of this region lead to dramatic effects and support the hypothesis that dimerization of ERR α DBD on DNA is intrinsically linked to the nature of DNA sequence. Since DNA groove dimensions depend on the DNA sequence (44–46), we used a high-throughput, experimentally well validated method to predict the DNA shape features of the sequences considered in

our studies (47). As **Figure 7** indicates, the analysis shows large differences in the minor groove widths between the *tff1* ERE/IR3 and embERRE/IR3 right in the region between positions (+5) and (+9). The embERRE/IR3 exhibits a pronounced minimum around the nucleotide at position (+6), while the *tff1* ERE/IR3 behaves at contrary at this location with a peak maximum at positions (+6) and (+7). These observations suggest that a narrow minor groove between positions (+6) and (+9) is essential for the stabilization of ERR α DBD homodimer and that wide and shallow minor groove at this location is not favorable to dimer formation. Next, we repeated the DNA shape prediction for the series of mutant and natural sequences. As shown on **Figure 7**, the mutants embmutT7A and IR3mutA7T follow a quite similar profile with the expected trend, the former exhibiting a shallower minimum as compared to embERRE/IR3 and the latter a strong decrease in the minor groove width as compared to *tff1* ERE/IR3. These predictions are consistent with the observations of the destabilization of the dimeric form for embmutT7A, or on the contrary of stabilization of a fraction of the complex into the dimeric form for IR3mutA7T. Remarkably, the DNA shape predictions for the various individual ERR binding sites considered in our studies are remarkably consistent with the observations of dimer versus monomer-only behavior (see Figure S8 in Supplementary Material).

DISCUSSION

Previous studies established that the ERRs function as homodimers. In particular, dimerization is required for the transcriptional activity of these receptors (48–51) and for the productive interaction with coactivators (10, 42, 52). The LBD was shown to mediate, in a large part, dimerization and the crystal structures of the ERRs (25, 26, 53–55) demonstrated in a consistent manner that the ERR LBD homodimer has a canonical dimerization interface, similar to the one seen in other NR homo- and heterodimers (56, 57). Concerning the DNA-binding properties, the ERR can bind *in vitro* as a homodimer to palindromic IR3 REs, such as those recognized by the ER (16, 42). However, *in vivo*, the ERR-binding sites are monomeric sites composed of extended half-site sequences (ERRE), and no consensus can be found for a second-binding site (12, 14). In addition, it was suggested that the sequence of the ERRE, and in particular that of the 3-bp extension, dictates the binding preference of ERR as a dimer or as a monomer even though only the dimeric form, and not the monomeric one, was shown to be capable of interacting with the

FIGURE 6 | Continued

Biochemical and biophysical analysis of DNA mutants suggest that the 3'-end region is crucial for dimer stabilization. **(A)** Nucleotide sequence of the 26-bp DNA mutants, Pu, destabPu, IR3mutA7A, embmutT7A, and 3'IR3TAA. In red are highlighted the changes compared to the parent wild-type sequence. The numbering of the nucleotides is indicated below the DNA sequence. **(B)** Ammonia/CAPS polyacrylamide gel of the complexes for a 1:2 DNA:protein ratio. The complexes, numbered from 1 to 10 are described in the table on the right-hand side. D and M stand for dimer and monomer, respectively. Notice the appearance of aspecific oligomeric species for higher DNA:protein ratios (marked by a star) for some of the DNAs. **(C)** Size-exclusion chromatography (SEC)-MALS analysis of ERR α DNA-binding domain (DBD) bound to emberERRE/IR3, *tff1* ERE/IR3, destabPu, and embmutT7A (160 μ M) showing the elution profile on a SEC S75 10/300 with the direct molar mass measurement of each elution peak. Mutating emberERRE/IR3 at (+7) to (+9), by adding the sequence found in *tff1* ERE/IR3 (in destabPu) or by changing T to A (embmutT7A) leads to the destabilization of the dimeric form of ERR α DBD on DNA (as suggested by the green arrow). On the right-hand side: ammonia/CAPS polyacrylamide gel of ERR α DBD bound to emberERRE/IR3 (wt, lanes 1, 2) and embmutT7A (mut, lanes 3, 4) for (1:1) (lanes 1, 3) and (0.5:1) (lanes 2, 4) DNA:protein ratios. D and M stand for dimer and monomer, respectively. Notice the appearance of aspecific oligomeric species for higher DNA:protein ratios (marked by a star). **(D)** Ammonia/CAPS polyacrylamide gel of the complexes after size-exclusion chromatography. The elution peak was fractionated in 40 μ L fractions and the fraction corresponding to the maximum of the peak was retained for native gel chromatographic analysis. D and M stand for dimer and monomer, respectively. The complexes, numbered from 1 to 8 are described in the table on the right-hand side.

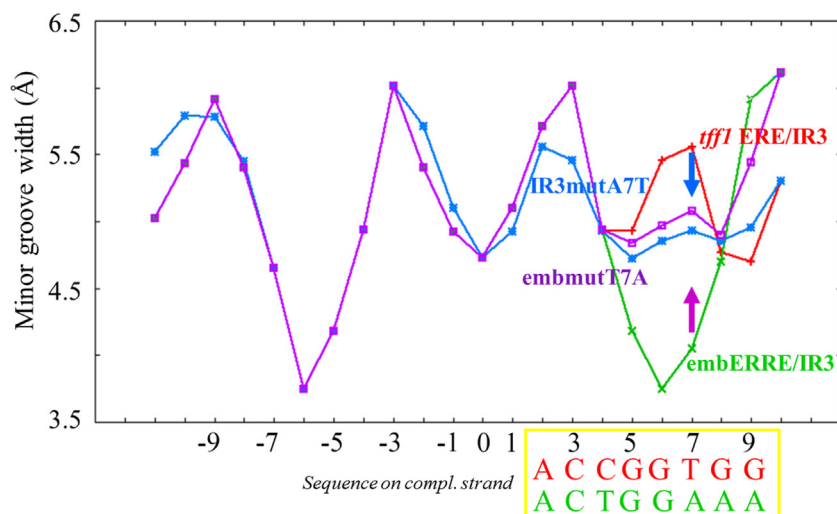


FIGURE 7 | DNA shape predictions of emberERRE and *tff1* ERE/IR3 and their respective point DNA mutant embmutT7A and IR3mutA7T. Minor groove width (Å) is plotted as a function of base sequence for emberERRE/IR3 (green), *tff1* ERE/IR3 (red), embmutT7A (purple), and IR3mutA7T (blue). The position of the bases is given with respect to the central base pair of the spacer (position 0). The sequences of the complementary strand of *tff1* ERE/IR3 (red) and emberERRE/IR3 (green) are given for positions (+2) to (+9) and comprise the second half-site and the two first flanking nucleotides. The purple arrow indicates the destabilization in the dimer formation seen for ERR α DNA-binding domain-emberERRE when position (+7) is affected (embmutT7A), while the blue arrow indicates a partial stabilization of dimer formation when *tff1* ERE/IR3 is point-mutated by introducing an T/A at position (+7), resulting to IR3mutA7T.

coactivator PGC-1 α (10, 42, 51). Thus, the mode of binding of DNA by ERR remained elusive and controversial.

To study the molecular mechanisms of binding and recognition of DNA by ERR, we decided to focus on the DNA-binding mode of the isolated DBD, allowing an unbiased understanding of the intrinsic DNA-binding properties of the protein, independently of the dimerization of the LBD. Using a combined approach of complementary biophysical and structural techniques, we show that ERR α DBD behaves either as a monomer or as a dimer depending on the DNA sequence. This is the first report demonstrating that an ERR α DBD dimer can be formed on DNA and that the dimerization of the DBD is not linked to the mere existence of two hexameric half-sites in the binding sequence onto which the two subunits could reside. We indeed show that on classical IR3 RE, such as the *tff1* ERE/IR3 element, ERR α DBD binds as a monomer, in contrast to what is observed for ER DBD that dimerizes in a strong cooperative manner on this RE (31, 35, 58).

We demonstrate the existence of ERR α DBD homodimer on the emberERRE/IR3 binding site which is composed of an extended half-site embedded into an IR3 RE. Binding on this element is observed for different lengths of DNA, indicating that the effect is not biased by a specific oligonucleotide. On the other hand, the fact that the sequence is composed of an extended half-site RE embedded into an IR3 element is not the key requirement that leads to the presence of a homodimer. Importantly, the homodimer can form on different types of REs, i.e., on *rb1cc1* IR3, on *tff1* ERRE, or on emberERRE/IR3 and what counts for dimerization, as demonstrated by the studies on the chimera DNAs, is the sequence at the 3'-end where the second ERR α DBD subunit can potentially bind. The analysis of the region of emberERRE/IR3, where the second subunit binds, reveals a T/A-rich region of the first three nucleotides of the second half-site on the complementary strand and the two flanking bases (+5-GGAA-+9). Mutating this region of emberERRE/IR3 by introducing an A/T bp at position (+7) leads to the destabilization of the dimeric form

(destabPu and embmutT7A). Conversely, mutating the equivalent region of *tff1* ERE/IR3 (+5-GGTGG-+9) to purines only (Pu or IR3mutA7T) leads to a remarkable stabilization of the complex into the dimeric form.

The specific recognition of DNA by proteins involves two mechanisms, one that relies on a specific sequence through base- and amino acid-specific hydrogen bonds and occurs primarily in the major groove and another one that involves sequence-dependent DNA shape effects, like minor groove width variations. Local sequence-dependent minor groove shape variations have indeed been established as a crucial mechanism widely used in the protein–DNA recognition that allows proteins to distinguish small differences in nucleotide sequence (44–46). Further, minor groove width and electrostatic potential are strongly correlated. Narrow minor grooves exhibit an enhanced electronegative potential and form specific binding sites for positively charged amino acids, and in particular for arginine residues. Using the DNA shape method (47) applied to the individual DNA sequences, we demonstrate that the minor groove width is intrinsically correlated to the capacity of the receptor DBD to homodimerize on DNA in an IR3-type of configuration (**Figure 7**; Figure S8 in Supplementary Material). Crucial nucleotides for dimerization effect are base pairs in the first half of the second binding site and flanking nucleotides. Our data parallel with the recent studies of GR DBD on different natural IR3 REs (GBSs) which report that the flanking nucleotides modulate DNA shape locally by acting on the minor groove width (59), but the extent of the variation in minor groove width seen for GBSs is rather modest as compared to that predicted for the ERR DNA-binding sequences. Interestingly, changing the flanking nucleotides of the GBSs resulted in different relative positioning of the dimer halves with consequences on the dimerization interface. The authors further argued that an intact GR dimerization interface driven by the sequence-dependent DNA shape is crucial for adequate positioning of the two GR subunits and that the functionally relevant positioning of the two subunits differs from the optimal positioning of the two DBDs in the major groove. Here, we show an even more striking effect, because the sequence-dependent DNA shape and the corresponding minor groove width at position (+5) to (+9) is a key factor in the stabilization of the ERR α DBD homodimer on DNA. The structure of the monomeric complex between ERR β DBD and a short 13-bp consensus recognition sequence of the type ERRE provides the structural bases for the stabilization of a monomer on ERRE, which was shown to strongly depend on additional contacts between residues in the A-box at the CTE, including the Arg–Gly–Gly–Arg motif, and the minor groove at the level of the 3-bp 5'-extension (24). In this article, we show that after the specific binding of the first ERR DBD subunit to the 9 bp ERRE, the dimerization of the second subunit will take place in a cooperative manner on DNA only if the local DNA shape and its intrinsic groove dimensions are adequate. From the analysis of the DNA shape as predicted for individual DNA sequences, we see that dimer formation is favored by a narrow minor groove. Indeed, the embERRE/IR3 sequence between position (+7) and (+9) exhibits an A-tract that favors a narrow minor groove. A-tracts have indeed been identified in a large

number of protein–DNA complexes to positively correlate with narrow minor (60) that represent the binding sites of positively charged arginine residues (45, 46). For example, the Hox family of homeodomain-containing transcription factors bind to generic binding sites through major groove-recognition helix interactions, but the specificity in target gene recognition arises from DNA shape and electrostatic potential driven interactions between the N-terminal arm and linker regions of the Hox protein with the minor groove (61), in a way very similar to the one observed here for ERR α DBD and its CTE.

The present studies demonstrate that the different ERR-binding sequences lead to different dimerization properties of the isolated ERR α DBD on DNA. This effect is correlated to the sequence-dependent DNA shape that represents an input signal that dictates the stabilization of the homodimer on DNA. Structure–function studies of GR DBD indicated there is no correlation between *in vitro* affinity and *in vivo* activity of this homodimer on specific DNA sequences (59). This is also the case for ERR, as suggested by *in vitro* binding affinity experiments, which indicate for example that ERR binds with high affinity to the *tff1* ERE/IR3, while exhibiting a weak transcriptional activity on this element (16, 42). However, our studies give further insight into the role of DNA shape which affects the dimerization capability of the isolated DBD.

The consequence for the binding of the full receptor which naturally forms a homodimer through the LBD is that one of the two DBD subunits is anchored in a specific manner to DNA, while the degree of stabilization of the other subunit on DNA depends on the DNA shape that it experiences. Thus, the conformation of the full homodimeric receptor and its dynamic behavior on DNA are likely to be affected. As a result, the interactions with co-regulators could be differentially modulated by providing distinct interactions surfaces. Previous studies on the binding of full ERR to DNA showed that indeed, depending on the sequence of the target elements, ERR exhibits differential affinity for the co-regulators PGC-1 and RIP14, which in turn alter its transcriptional activity (62). This is also the case for other NRs, which show that their binding sequence leads to a differential recruitment of co-regulators at target gene promoters, as e.g., for the ER (63).

In summary, our report demonstrates that the sequence-dependent DNA shape of the ERR-binding site influences the recruitment of ERR α DBD dimer on DNA, by promoting the right conformation of the two subunits on DNA for cooperative interaction and dimer stabilization. The key structural component promoting dimer formation is the local geometry of the minor groove that encompasses the second half-site and the flanking nucleotides. The local minor groove shape strongly depends on the sequence and it is this information imprinted in the DNA shape that ERR uses to achieve DNA-binding specificity (scheme **Figure 8**). It is tempting to speculate that DNA-binding specificity of other NRs to their target genes is achieved by similar regulatory mechanisms. In particular, the oxosteroid NR family, including the AR, the GR, the MR and the PR receptors bind as homodimer to similar IR3 binding sites that exhibit a well conserved and strong half-site and a second degenerated one that gives oxosteroid receptor specificity (4, 5, 7, 32, 64–66). Our

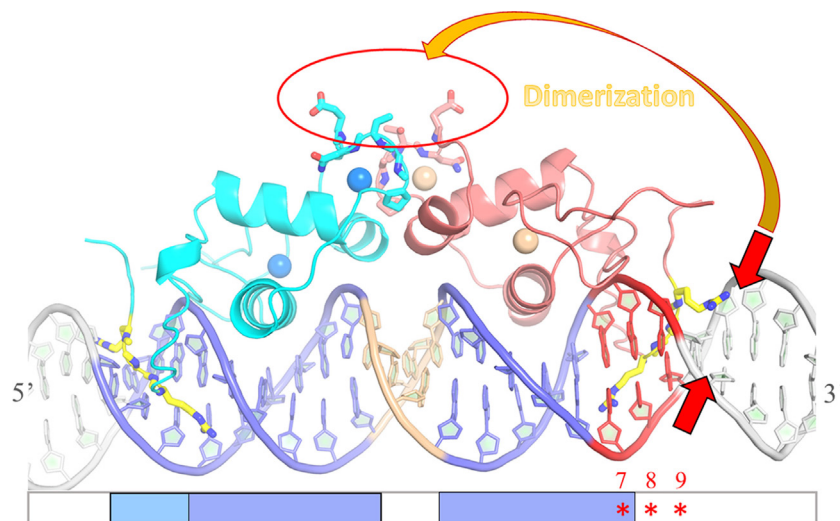


FIGURE 8 | Schematic drawing of the influence of DNA shape on dimer stabilization. Model of the ERR α DNA-binding domain (DBD) dimer on DNA based on the structure of ER α DBD-IR3 response elements (RE) (PDB code 1HCQ), where the nuclear magnetic resonance structure of ERR β DBD (PDB code 1L01) is superimposed to each of the two subunits of ER α DBD-IR3 RE. An ideal B-DNA model is used in the drawing. Comparative analysis of the residues of the D-box involved in dimerization between ER and ERR suggests that ERR α DBD could *a priori* dimerize in a way similar to that seen in the structure of ER α DBD, without any structural impediment (red circle). On the other hand, the stabilization of ERR α DBD dimer on DNA is influenced by the sequence-dependent DNA shape of the second ERR-binding site at the 3'-end of DNA. The local geometry of the minor groove that encompasses the second half-site and the flanking nucleotides (especially between positions +5 and +9) is crucial for the formation of an ERR α DBD dimer on DNA. Sequence-driven narrow minor grooves at this location (small red arrows) favor dimer stabilization (large orange arrow).

studies on ERR suggest that the local sequence-dependent DNA shape of the second half-site is crucial for receptor specificity in DNA recognition.

AUTHOR CONTRIBUTIONS

IB, DM, and BK designed the study and supervised research; IB, KM-A, and DM wrote the manuscript, KM-A, KT, MB, IH, IL, MT, and IB performed the experiments; KM-A, KT, MB, IL, SC, and IB analyzed data.

ACKNOWLEDGMENTS

The authors thank the Structural Biology and Genomics platform (IGBMC) for providing SEC-MALLS facility and support and Claude Ling for technical assistance. This work was supported by CNRS, INSERM, The Université de Strasbourg, the Association pour la Recherche sur le Cancer (ARC) and l'Alsace contre le Cancer. The authors acknowledge the support and the use of the French Infrastructure for Integrated Structural Biology FRISBI ANR-10-INSB-05 Instruct, a Landmark ESFRI project, the French Proteomic Infrastructure ProFI ANR-10-INBS-08-03 and the GIS IBiSA. KT acknowledges KaroBio Research Foundation and l'Alsace Contre le Cancer for funding of her Ph.D. fellowship. MB acknowledges the Région Alsace for funding of his Ph.D. fellowship. KM-A acknowledges the Fondation pour la Recherche Médicale for funding of his postdoctoral fellowship. The authors thank Vincent Giguère (McGill University Health Centre, Montréal, QC, Canada) for discussion at the initial stages of the project.

SUPPLEMENTARY MATERIAL

The Supplementary Material for this article can be found online at <http://journal.frontiersin.org/article/10.3389/fendo.2017.00140/full#supplementary-material>.

FIGURE S1 | Titration of *tff1* ERE/IR3 DNA by ERR α DNA-binding domain (DBD). Imino protons region of 1D spectra recorded at 20°C in 50 mM sodium phosphate buffer (pH 7), 5 mM MgCl₂ and 1 mM TCEP in 90/10 H₂O/D₂O. The assignments of imino proton based on NOESY experiments are indicated for free *tff1* ERE/IR3 (top). Tentative assignments are indicated in italics. The ratios (ERR α DBD: *tff1* ERE/IR3) are indicated on the left. Broken lines indicate imino protons that undergo chemical shift changes (red in the sequence) and lines indicate imino proton that remain unchanged (blue in the sequence).

FIGURE S2 | Titration of *lf* ERRE DNA by ERR α DNA-binding domain (DBD). Imino protons region of 1D spectra recorded at 20°C in 50 mM sodium phosphate buffer (pH 7.0), 5 mM MgCl₂ and 1 mM TCEP in 90/10 H₂O/D₂O. The assignments of imino proton based on NOESY experiments are indicated for free *lf* estrogen-related response element (ERRE) (top). The ratios (ERR α DBD: *lf* ERRE) are indicated on the left. Broken lines indicate imino protons that undergo chemical shift changes (red in the sequence) and lines indicate imino proton that remain unchanged (blue in the sequence).

FIGURE S3 | Titration of *tra* estrogen-related response element (ERRE) DNA by ERR α DNA-binding domain (DBD). Imino protons region of 1D spectra recorded at 20°C in 50 mM sodium phosphate buffer (pH 7.0), 5 mM MgCl₂ and 1 mM TCEP in 90/10 H₂O/D₂O. The assignments of imino proton based on NOESY experiments are indicated for free *tra* ERRE (top). The ratios (ERR α DBD: *tra* ERRE) are indicated on the left. Broken lines indicate imino protons that undergo chemical shift changes (red in the sequence) and lines indicate imino proton that remain unchanged (blue in the sequence).

FIGURE S4 | Titration of *rb1cc1* IR3 DNA by ERR α DNA-binding domain (DBD). Imino protons region of 1D spectra recorded at 20°C in 50 mM sodium phosphate buffer (pH 7.0), 5 mM MgCl₂, and 1 mM TCEP in 90/10 H₂O/D₂O. The assignments of imino proton based on NOESY experiments are indicated for free

rb1cc1/IR3 (top). The ratios (ERR α DBD: rbcc1 IR3) are indicated on the left. Broken lines indicate imino protons that undergo chemical shift changes (red in the sequence).

FIGURE S5 | Titration of embERRE/IR3 DNA by ERR α DNA-binding domain (DBD). Imino protons region of 1D spectra recorded at 20°C in 50 mM sodium phosphate buffer (pH 7.0), 5 mM MgCl₂, and 1 mM TCEP in 90/10 H₂O/D₂O. The assignments of imino proton based on NOESY experiments are indicated for free embERRE/IR3 (top). The ratios (ERR α DBD: embERRE/IR3) are indicated on the left. Broken lines indicate imino protons that undergo chemical shift changes (red in the sequence).

FIGURE S6 | Non-denaturing Mass Spectrometry analysis of free DNA. Non-denaturing mass spectrometry analysis of free DNA complexes for (A) embERRE/IR3, (B) 5'ttf, and (C) 5'emb, all being 26 bps long, recorded in the same non-denaturing conditions as the protein-DNA complexes are measured (Pi = 6 mbar; Vc = 140V). The charged states are indicated above the peaks. A small fraction of DNA dimer is observed under these experimental conditions.

FIGURE S7 | Size-exclusion chromatography-coupled multi-angle laser light scattering of ERR α DNA-binding domain (DBD)-DNA complexes. SEC-MALLS analysis of ERR α DBD bound to 26 bp embERRE/IR3 (blue), ttf1 ERE/IR3 (red), embmutT7A (green), IR3mutA7T (cyan), and Pu (dark blue) (160 μ M), showing the elution profile on a SEC S75 10/300 with the direct molar mass measurement of each elution peak. The elution profiles of the complexes with the mutant DNA complexes are eluted slightly earlier as ttf1 ERE/IR3-ERR α DBD and the fraction

of complex collected at the peak maximum is seen to contain a small fraction of dimeric DBD on DNA (see **Figure 6D**).

FIGURE S8 | DNashape predictions of other DNA fragments. Minor groove width (Å) is plotted as a function of base sequence for (A) rb1cc1 IR3 (blue) and compared to those of embERRE/IR3 (green) and ttf1 ERE/IR3 (red). The position of the bases is given with respect to the central bp of the spacer (position 0). The sequences of the complementary strand of rb1cc1 IR3 (blue) and embERRE/IR3 (green) are given for positions (+2) to (+9) and comprise the second half-site and the two first flanking nucleotides; (B) tra estrogen-related response element (ERRE) (blue) and ttf1 ERRE (green) compared to those of embERRE/IR3 (red). The position of the bases is given with respect to the central bp of the spacer (position 0). The sequences of the complementary strand of tra ERRE (blue) and ttf1 ERRE (green) are given for positions (+2) to (+9) and comprise the second half-site and the two first flanking nucleotides; (C) abcc5 ERRE/IR3 (blue) and compared to those of embERRE/IR3 (green) and ttf1 ERE/IR3 (red). The position of the bases is given with respect to the central bp of the spacer (position 0). The sequences of the complementary strand of abcc5 ERRE/IR3 (blue) and embERRE/IR3 (green) are given for positions (+2) to (+9) and comprise the second half-site and the two first flanking nucleotides; (D) the mutants destabPu (blue) and Pu (purple) and compared to those of embERRE/IR3 (green) and ttf1 ERE/IR3 (red). The position of the bases is given with respect to the central bp of the spacer (position 0). The sequences of the complementary strand of destabPu (blue) and Pu (purple) are given for positions (+2) to (+9) and comprise the second half-site and the two first flanking nucleotides.

REFERENCES

- Gronemeyer H, Gustafsson JA, Laudet V. Principles for modulation of the nuclear receptor superfamily. *Nat Rev Drug Discov* (2004) 3:950–64. doi:10.1038/nrd1551
- Laudet V, Gronemeyer H. *The Nuclear Receptor Factsbook*. London: Academic Press (2002).
- Huang P, Chandra V, Rastinejad F. Structural overview of the nuclear receptor superfamily: insights into physiology and therapeutics. *Annu Rev Physiol* (2010) 72:247–72. doi:10.1146/annurev-physiol-021909-135917
- Helsen C, Claessens F. Looking at nuclear receptors from a new angle. *Mol Cell Endocrinol* (2014) 382:97–106. doi:10.1016/j.mce.2013.09.009
- Helsen C, Kerkhofs S, Clinckemalie L, Spans L, Laurent M, Boonen S, et al. Structural basis for nuclear hormone receptor DNA binding. *Mol Cell Endocrinol* (2011) 348:411–7. doi:10.1016/j.mce.2011.07.025
- Aagaard MM, Siersbmk R, Mandrup S. Molecular basis for gene-specific transactivation by nuclear receptors. *Biochim Biophys Acta* (2010) 1812:824–35. doi:10.1016/j.bbadis.2010.12.018
- Rastinejad F, Huang P, Chandra V, Khorasanizadeh S. Understanding nuclear receptor form and function using structural biology. *J Mol Endocrinol* (2013) 51(3):T1–21. doi:10.1530/JME-13-0173
- Khorasanizadeh S, Rastinejad F. Nuclear-receptor interactions on DNA-response elements. *Trends Biochem Sci* (2001) 26:384–90. doi:10.1016/S0968-0004(01)01800-X
- Johnston SD, Liu X, Zuo F, Eisenbraun TL, Wiley SR, Kraus RJ, et al. Estrogen-related receptor {alpha}1 functionally binds as a monomer to extended half-site sequences including ones contained within estrogen-response elements. *Mol Endocrinol* (1997) 11:342–52. doi:10.1210/mend.11.3.9897
- Barry JB, Laganieri J, Giguere V. A single nucleotide in an estrogen-related receptor {alpha} site can dictate mode of binding and peroxisome proliferator-activated receptor {gamma} coactivator 1{alpha} activation of target promoters. *Mol Endocrinol* (2006) 20:302–10. doi:10.1210/me.2005-0313
- Sladek R, Bader JA, Giguere V. The orphan nuclear receptor estrogen-related receptor alpha is a transcriptional regulator of the human medium-chain acyl coenzyme A dehydrogenase gene. *Mol Cell Biol* (1997) 17:5400–9. doi:10.1128/MCB.17.9.5400
- Deblois G, Hall JA, Perry MC, Laganieri J, Ghahremani M, Park M, et al. Genome-wide identification of direct target genes implicates estrogen-related receptor alpha as a determinant of breast cancer heterogeneity. *Cancer Res* (2009) 69:6149–57. doi:10.1158/0008-5472.CAN-09-1251
- Deblois G, St-Pierre J, Giguere V. The PGC-1/ERR signaling axis in cancer. *Oncogene* (2013) 32(30):3483–90. doi:10.1038/onc.2012.529
- Dufour CR, Wilson BJ, Huss JM, Kelly DP, Alaynick WA, Downes M, et al. Genome-wide orchestration of cardiac functions by the orphan nuclear receptors ERR[alpha] and [gamma]. *Cell Metab* (2007) 5:345–56. doi:10.1016/j.cmet.2007.03.007
- Xie W, Hong H, Yang NN, Lin RJ, Simon CM, Stallcup MR, et al. Constitutive activation of transcription and binding of coactivator by estrogen-related receptors 1 and 2. *Mol Endocrinol* (1999) 13:2151–62. doi:10.1210/mend.13.12.0381
- Lu D, Kiriya Y, Lee KY, Giguere V. Transcriptional regulation of the estrogen-inducible pS2 breast cancer marker gene by the ERR family of orphan nuclear receptors. *Cancer Res* (2001) 61:6755–61.
- Huss JM, Garbacz W, Xie W. Constitutive activities of estrogen-related receptors: transcriptional regulation of metabolism by the ERR pathways in health and disease. *Biochim Biophys Acta* (2015) 1852(9):1912–27. doi:10.1016/j.bbadis.2015.06.016
- Audet-Walsh E, Giguere V. The multiple universes of estrogen-related receptor [alpha] and [gamma] in metabolic control and related diseases. *Acta Pharmacol Sin* (2015) 36:51–61. doi:10.1038/aps.2014.121
- Deblois G, Giguere V. Oestrogen-related receptors in breast cancer: control of cellular metabolism and beyond. *Nat Rev Cancer* (2013) 13:27–36. doi:10.1038/nrc3396
- Deblois G, Giguere V. Functional and physiological genomics of estrogen-related receptors (ERRs) in health and disease. *Biochim Biophys Acta* (2011) 1812:1032–40. doi:10.1016/j.bbadis.2010.12.009
- Giguere V. Transcriptional control of energy homeostasis by the estrogen-related receptors. *Endocr Rev* (2008) 29:677–96. doi:10.1210/er.2008-0017
- Giguere V, Dufour CR, Eichner LJ, Deblois G, Cermakian N. Estrogen-related receptor alpha, the molecular clock, and transcriptional control of metabolic outputs. *Cold Spring Harb Symp Quant Biol* (2011) 76:57–61. doi:10.1101/sqb.2011.76.011031
- Wang T, McDonald C, Petrenko NB, Leblanc M, Wang T, Giguere V, et al. ERRalpha and ERRgamma are essential coordinators of cardiac metabolism and function. *Mol Cell Biol* (2015) 35(7):1281–98. doi:10.1128/MCB.01156-14
- Gearhart MD, Holmbeck SM, Evans RM, Dyson HJ, Wright PE. Monomeric complex of human orphan estrogen related receptor-2 with DNA: a pseudo-dimer interface mediates extended half-site recognition. *J Mol Biol* (2003) 327:819–32. doi:10.1016/S0022-2836(03)00183-9
- Greschik H, Althage M, Flaig R, Sato Y, Chavand V, Peluso-Iltis C, et al. Communication between the ERRalpha homodimer interface and the PGC-1alpha binding surface via the helix 8-9 loop. *J Biol Chem* (2008) 283:20220–30. doi:10.1074/jbc.M801920200

26. Greschik H, Wurtz J-M, Sanglier S, Bourguet W, van Dorselaer A, Moras D, et al. Structural and functional evidence for ligand-independent transcriptional activation by the estrogen-related receptor 3. *Mol Cell* (2001) 9:303–13. doi:10.1016/S1097-2765(02)00444-6
27. Kallen J, Lattmann R, Beerli R, Blechschmidt A, Blommers MJJ, Geiser M, et al. Crystal structure of human estrogen-related receptor {alpha} in complex with a synthetic inverse agonist reveals its novel molecular mechanism. *J Biol Chem* (2007) 282:23231–9. doi:10.1074/jbc.M703337200
28. Kallen J, Schlaeppi JM, Bitsch F, Filipuzzi I, Schilb A, Riou V, et al. Evidence for ligand-independent transcriptional activation of the human estrogen-related receptor alpha (ERRalpha): crystal structure of ERRalpha ligand-binding domain in complex with peroxisome proliferator-activated receptor coactivator-1alpha. *J Biol Chem* (2004) 279:49330–7. doi:10.1074/jbc.M407999200
29. Wang L, Zuercher WJ, Conler TG, Lambert MH, Miller AB, Orband-Miller LA, et al. X-ray crystal structures of the estrogen related receptor-gamma ligand binding domain in three functional states reveal the molecular basis of small molecule regulation. *J Biol Chem* (2006) 281:37773–81. doi:10.1074/jbc.M608410200
30. Sem DS, Casimiro DR, Klierer SA, Provençal J, Evans RM, Wright PE. NMR spectroscopic studies of the DNA-binding domain of the monomer-binding nuclear orphan receptor, human estrogen related receptor-2. *J Biol Chem* (1997) 272:18038–43. doi:10.1074/jbc.272.29.18038
31. Nardulli AM, Lew D, Erijman L, Shapiro DJ. Purified estrogen receptor DNA binding domain expressed in *Escherichia coli* activates transcription of an estrogen-responsive promoter in cultured cells. *J Biol Chem* (1991) 266:24070–6.
32. Denayer S, Helsen C, Thorrez L, Haelens A, Claessens F. The rules of DNA recognition by the androgen receptor. *Mol Endocrinol* (2010) 24:898–913. doi:10.1210/me.2009-0310
33. Luisi BF, Xu WX, Otwinowski Z, Freedman LP, Yamamoto KR, Sigler PB. Crystallographic analysis of the interaction of the glucocorticoid receptor with DNA. *Nature* (1991) 352:497–505. doi:10.1038/352497a0
34. Meijnsing SH, Pufall MA, So AY, Bates DL, Chen L, Yamamoto KR. DNA binding site sequence directs glucocorticoid receptor structure and activity. *Science* (2009) 324:407–10. doi:10.1126/science.1164265
35. Schwabe JWR, Chapman L, Finch JT, Rhodes D. The crystal structure of the estrogen receptor DNA-binding domain bound to DNA: how receptors discriminate between their response elements. *Cell* (1993) 75:567–78. doi:10.1016/0092-8674(93)90390-C
36. Goddard T, Kneller D. SPARKY3. San Francisco: University of California (2004). Available from: <https://www.cgl.ucsf.edu/home/sparky/>
37. Sklenar V, Piotto M, Leppik R, Saudek V. Gradient-tailored water suppression for 1H-15N HSQC experiments optimized to retain full sensitivity. *J Magn Reson A* (1993) 102:241–5. doi:10.1006/jmra.1993.1098
38. Plateau P, Gueron M. Exchangeable proton NMR without base-line distortion, using new strong-pulse sequences. *J Am Chem Soc* (1982) 104:7310–1. doi:10.1021/ja00389a067
39. Piotto M, Saudek V, Sklenář V. Gradient-tailored excitation for single-quantum NMR spectroscopy of aqueous solutions. *J Biomol NMR* (1992) 2:661–5. doi:10.1007/BF02192855
40. Yang N, Shigetani H, Shi H, Teng CT. Estrogen-related receptor, hERR1, modulates estrogen receptor-mediated response of human lactoferrin gene promoter. *J Biol Chem* (1996) 271:5795–804. doi:10.1074/jbc.271.10.5795
41. Vanacker JM, Bonnelye E, Delmarre C, Laudet V. Activation of the thyroid hormone receptor alpha gene promoter by the orphan nuclear receptor ERR alpha. *Oncogene* (1998) 17:2429–35. doi:10.1038/sj.onc.1202167
42. Barry JB, Giguere V. Epidermal growth factor-induced signaling in breast cancer cells results in selective target gene activation by orphan nuclear receptor estrogen-related receptor {alpha}. *Cancer Res* (2005) 65:6120–9. doi:10.1158/0008-5472.CAN-05-0922
43. Akter M, Chano T, Okabe H, Yamaguchi T, Hirose F, Osumi T. Target specificities of estrogen receptor-related receptors: analysis of binding sequences and identification of Rb1-inducible coiled-coil 1 (Rb1cc1) as a target gene. *J Biochem* (2008) 143:395–406. doi:10.1093/jb/mvm231
44. Oguey C, Foppe N, Hartmann B. Understanding the sequence-dependence of DNA groove dimensions: implications for DNA interactions. *PLoS One* (2011) 5:e15931. doi:10.1371/journal.pone.0015931
45. Rohs R, Jin X, West SM, Joshi R, Honig B, Mann RS. Origins of specificity in protein-DNA recognition. *Annu Rev Biochem* (2010) 79:233–69. doi:10.1146/annurev-biochem-060408-091030
46. Rohs R, West SM, Sosinsky A, Liu P, Mann RS, Honig B. The role of DNA shape in protein-DNA recognition. *Nature* (2009) 461:1248–53. doi:10.1038/nature08473
47. Zhou T, Yang L, Lu Y, Dror I, Dantas Machado AC, Ghane T, et al. DNashape: a method for the high-throughput prediction of DNA structural features on a genomic scale. *Nucleic Acids Res* (2013) 41:W56–62. doi:10.1093/nar/gkt437
48. Liu X, Nishimura H, Fujiyama A, Matsushima A, Shimohigashi M, Shimohigashi Y. α -Helix-peptides comprising the human nuclear receptor ERR γ competitively provoke inhibition of functional homomeric dimerization. *Pept Sci* (2016) 106:547–54. doi:10.1002/bip.22795
49. Hentschke M, Süsens U, Borgmeyer U. Domains of ERR γ that mediate homodimerization and interaction with factors stimulating DNA binding. *Eur J Biochem* (2002) 269:4086–97. doi:10.1046/j.1432-1033.2002.03102.x
50. Huppunen J, Aarnisalo P. Dimerization modulates the activity of the orphan nuclear receptor ERR γ . *Biochem Biophys Res Commun* (2004) 314:964–70. doi:10.1016/j.bbrc.2003.12.194
51. Horard B, Castet A, Bardet PL, Laudet V, Cavailles V, Vanacker JM. Dimerization is required for transactivation by estrogen-receptor-related (ERR) orphan receptors: evidence from amphioxus ERR. *J Mol Endocrinol* (2004) 33:493–509. doi:10.1677/jme.1.01538
52. Takacs M, Petoukhov MV, Atkinson RA, Roblin P, Ogi FX, Demeler B, et al. The asymmetric binding of PGC-1 α to the ERRalpha and ERRgamma nuclear receptor homodimers involves a similar recognition mechanism. *PLoS One* (2013) 8:e67810. doi:10.1371/journal.pone.0067810
53. Greschik H, Flaig R, Renaud JP, Moras D. Structural basis for the deactivation of the estrogen-related receptor {gamma} by diethylstilbestrol or 4-hydroxytamoxifen and determinants of selectivity. *J Biol Chem* (2004) 279:33639–46. doi:10.1074/jbc.M402195200
54. Matsushima A, Teramoto T, Okada H, Liu X, Tokunaga T, Kakuta Y, et al. ERRgamma tethers strongly bisphenol A and 4-alpha-cumylphenol in an induced-fit manner. *Biochem Biophys Res Commun* (2008) 373:408–13. doi:10.1016/j.bbrc.2008.06.050
55. Liu X, Matsushima A, Okada H, Shimohigashi Y. Distinction of the binding modes for human nuclear receptor ERR{gamma} between bisphenol A and 4-hydroxytamoxifen. *J Biochem* (2010) 148(2):247–54. doi:10.1093/jb/mvq056
56. Billas I, Moras D. Allosteric controls of nuclear receptor function in the regulation of transcription. *J Mol Biol* (2013) 425:2317–29. doi:10.1016/j.jmb.2013.03.017
57. Moras D, Billas IML, Rochel N, Klaholz BP. Structure-function relationships in nuclear receptors: the facts. *Trends Biochem Sci* (2015) 40:287–90. doi:10.1016/j.tibs.2015.03.009
58. Kuntz MA, Shapiro DJ. Dimerizing the estrogen receptor DNA binding domain enhances binding to estrogen response elements. *J Biol Chem* (1997) 272:27949–56. doi:10.1074/jbc.272.44.27949
59. Schöne S, Jurk M, Helabad MB, Dror I, Lebars I, Kieffer B, et al. Sequences flanking the core-binding site modulate glucocorticoid receptor structure and activity. *Nat Commun* (2016) 7:12621. doi:10.1038/ncomms12621
60. Haran TE, Mohanty U. The unique structure of A-tracts and intrinsic DNA bending. *Q Rev Biophys* (2009) 42:41–81. doi:10.1017/S0033583509004752
61. Joshi R, Passner JM, Rohs R, Jain R, Sosinsky A, Crickmore MA, et al. Functional specificity of a Hox protein mediated by the recognition of minor groove structure. *Cell* (2007) 131:530–43. doi:10.1016/j.cell.2007.09.024
62. Sanyal S, Matthews J, Bouton D, Kim HJ, Choi HS, Treuter E, et al. Deoxyribonucleic acid response element-dependent regulation of transcription by orphan nuclear receptor estrogen receptor-related receptor {gamma}. *Mol Endocrinol* (2004) 18:312–25. doi:10.1210/me.2003-0165
63. Hall JM, McDonnell DP, Korach KS. Allosteric regulation of estrogen receptor structure, function, and coactivator recruitment by different estrogen response elements. *Mol Endocrinol* (2002) 16:489–86. doi:10.1210/mend.16.3.0814
64. Schoenmakers E, Verrijdt G, Peeters B, Verhoeven G, Rombauts W, Claessens F. Differences in DNA binding characteristics of the androgen and glucocorticoid receptors can determine hormone-specific responses. *J Biol Chem* (2000) 275:12290–7. doi:10.1074/jbc.275.16.12290
65. Sahu B, Pihlajamäa P, Dubois V, Kerkhofs S, Claessens F, Janne OA. Androgen receptor uses relaxed response element stringency for selective chromatin binding and transcriptional regulation in vivo. *Nucleic Acids Res* (2014) 42:4230–40. doi:10.1093/nar/gkt1401

66. Wilson S, Qi J, Filipp FV. Refinement of the androgen response element based on ChIP-Seq in androgen-insensitive and androgen-responsive prostate cancer cell lines. *Sci Rep* (2016) 6:32611. doi:10.1038/srep32611

Conflict of Interest Statement: The authors declare that the research was conducted in the absence of any commercial or financial relationships that could be construed as a potential conflict of interest.

Copyright © 2017 Mohideen-Abdul, Tazibt, Bourguet, Hazemann, Lebars, Takacs, Cianfèrari, Klaholz, Moras and Billas. This is an open-access article distributed under the terms of the Creative Commons Attribution License (CC BY). The use, distribution or reproduction in other forums is permitted, provided the original author(s) or licensor are credited and that the original publication in this journal is cited, in accordance with accepted academic practice. No use, distribution or reproduction is permitted which does not comply with these terms.